Balanced interferometric system for stability measurements

Jonathan D. Ellis,* Ki-Nam Joo, Jo W. Spronck, and Robert H. Munnig Schmidt
PME: Mechatronic System Design, Delft University of Technology, Mekelweg 2, 2628 CD Delft, The Netherlands
*Corresponding author: j.d.ellis@tudelft.nl

Received 24 November 2008; revised 9 February 2009; accepted 10 February 2009;
posted 11 February 2009 (Doc. ID 104483); published 16 March 2009

We describe two different, double-sided interferometer designs for measuring material stability. Both designs are balanced interferometers where the only optical path difference is the sample and the reference beams are located within the interferometer. One interferometer is a double-pass design, whereas the other is a single-pass system. Based on a tolerancing analysis, the single-pass system is less susceptible to initial component misalignment and motions during experiments. This single-pass interferometer was tested with an 86 nm thin-film silver sample for both short-term repeatability and long-term stability. In 66 repeatability tests of 30 min each, the mean measured drift rate was less than 1 pm/h rms. In two long-term tests (>9 h), the mean drift rate was less than 1.1 pm/h, which shows good agreement between the short- and long-term measurements. In these experiments, the mean measured length change was 2 nm rms. © 2009 Optical Society of America
OCIS codes: 120.3180, 120.0120, 120.3940.

1. Introduction

Tolerances on components for high-precision instruments are becoming increasingly tighter, not only for manufacturing, but also for their performance within a system. This encompasses a wide variety of instrument types, from lithography machines to space telescopes. The common link between these systems is their inherent complexity and their reliance on highly accurate parts to perform a process effectively. Until recently, most systems were designed with only limited considerations of a component's stability because the environmental effects were orders of magnitude higher. With better environmental control, this gap between environmental effects and stability effects becomes blurred. Thus, to increase the limits of precision instruments, more information is needed on material stability. This will provide useful insight into designing systems to have more inherent stability, leading to better accuracy.

Material stability is a difficult parameter to assess because the instrument that measures the stability will also have instabilities. For shorter time scales, such as in a lithography process, the stability of materials and thus of the instrument limits the time between calibrations and decreases output. Also, long-term stability is not critical for lithography because it performs relative processes that are zeroed every few minutes or less. However, the long-term stability becomes significant for metrology instruments, which are typically calibrated annually, and for space instruments, which must be, in many instances, operational for decades and have a no-maintenance requirement. Stability is particularly important for segmented mirror telescopes, which typically have a production run that spans years. Assessing the stability of these mirrored surfaces is critical because the large time-scale difference will cause different surface relaxation rates.

An instrument is, therefore, needed to measure material stability where the measurement is insensitive to the instrument's instability. With this instrument, relative material stability can be investigated, such as determining which material is more stable in a specific measurement environment. Quantifying an absolute stability parameter is important because it can confirm or disprove theoretical research on

0003-6935/09/091733-08$15.00/0
© 2009 Optical Society of America

atomic structuring [1], the stability of kinematic assemblies such as v-groove and sphere contacts [2], and atmospheric-to-vacuum transitions in materials [3]. In this paper, design considerations for two balanced interferometers to measure material stability are presented, as well as some preliminary testing results.

2. Instrument Specification

A measurement system with high resolution and a low contribution of measurement uncertainty is required for the investigation of material stability. Initially, samples with a length up to 50 mm long will be investigated. The final target of this research is to determine both short-term and long-term stability. Measurements will ultimately be assessed for 1 *h* intervals (short term) with a targeted uncertainty of 10 pm ($k = 2$) and up to a maximum of 4 weeks (long term) with a targeted uncertainty of 100 pm ($k = 2$). Additionally, these requirements are for samples measured both in air and in vacuum. The goal for this paper is to determine whether the proposed interferometers have the potential to achieve these final targets.

This instrument will use heterodyne interferometry because it is directly traceable to the length standard and is easily scalable for longer samples. As a trade-off, nonreflective samples will require an added reflective coating and thus will have a higher uncertainty. Last, this research will focus on instruments that perform double-sided measurements. Previous research into dilatometry has shown several single- and double-sided designs that may be applicable for stability measurements. Using a double-sided design removes two critical uncertainty contributors: mounting the sample to the reference plate, and characterizing the interaction between the sample and the reference plate.

The typical method to mount the sample is to wring it to a reference flat, which has been shown to contribute considerable measurement uncertainty [4,5]. This is a particular problem for single-sided instruments by, for example, Bennett [6], Birch [7], Okaji and Imai [8], and Schödel [5]. Several double-sided instruments have been developed that alleviate this problem; however, these still have additional problems that need to be resolved. These include a contact-based measurement causing additional instability [9]; a secondary reference, which allows only relative measurements [10]; and a wide diameter beam, which will be more subject to refractive index changes [4]. This research will focus on designing an instrument that is not subject to the aforementioned additional uncertainty contributors [11].

3. Double-Pass Interferometer

The initial interferometer analyzed is based on a double-pass dilatometer design by Ren *et al.* [12]. This interferometer has been modified, which is shown in Fig. 1, to incorporate the reference beams within the interferometer. The reference beams were

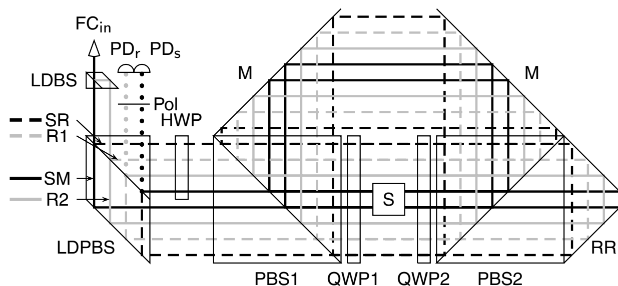

Fig. 1. Double-pass, double-sided interferometer for measuring sample length changes. Including the reference beam within the interferometer reduces the effects of polarization mixing and component misalignments. PD_s, PD_r, photodetectors.

incorporated within the interferometer to reduce the effects of misalignment on the measurement [13]. The input beam in this interferometer is a two-frequency source with linearly, orthogonally polarized electric fields. The input beam is split equally by a lateral displacement 50% beam splitter (LDBS). The beam that passes through the LDBS is then split by polarization states by a lateral displacement polarizing beam splitter (LDPBS). The LDPBS transmitted beam is the sample measurement (SM) beam, and the LDPBS reflected beam is the sample reference (SR) beam.

The SM beam passes through a polarizing beam splitter (PBS1), through a quarter-wave plate (QWP1), and reflects off the sample (S). It passes through QWP1 a second time, which then causes the beam to reflect off PBS1, then two mirrors (M), and then off a second polarizing beam splitter (PBS2). It then passes through another quarter-wave plate (QWP2), reflects off the sample, and then through QWP2 a second time. It then passes through PBS2, reflects off the retroreflector (RR), through PBS2 and QWP2 to hit the sample a third time. It then passes through QWP2, reflects off PBS2, two mirrors, PBS1, and then passes through QWP1. It reflects off the sample a fourth time, then passes through QWP1, PBS1, a half-wave plate (HWP) and then reflects from the LDPBS.

The SR beam passes through the HWP, PBS1, QWP1, and QWP2. When it passes through QWP2, its polarization is changed by 90°. It then reflects off PBS2, both mirrors, and PBS1, and then passes through QWP1, QWP2, and then PBS2. The SR beam then reflects off the retroreflector and passes back through PBS2, QWP2, and QWP1, where it then reflects off PBS1. This beam then reflects off the two mirrors, PBS2, and then passes through QWP2, QWP1, PBS1, and reflects off a mirror in the LDPBS. The SR beam then passes through the LDPBS, where it interferes with the SM beam by use of a polarizer (Pol), and the signal is then detected.

The LDBS reflected beam becomes the reference signal. The reference signal travels to the LDPBS, where it is also split by polarization into two different reference beams, R1 and R2. The R1 beam reflects off

the LDPBS and passes through a HWP at which point it has the same polarization state as R2 before PBS1. From this point, the paths between R1 and R2 are identical to the SR beam traveling back to the LDPBS. When traveling back to the LDPBS, the R2 beam then passes through the HWP. The R1 and R2 beams are interfered using the same polarizer as the SM and SR beams.

Although complicated, the optical path difference (OPD) between the SM and SR beams is the sample length times the optical resolution, which is a factor of four in this interferometer. Placing the reference beams in the interferometer reduces the stacking effect of tolerances, specifically with polarizing components. A Jones matrix model was implemented to determine alignment sensitivity and compensation of polarizing components in this interferometer. This is particularly important because this interferometer has a long optical path length and the light passes through numerous polarizing components. The matrix model describing the interferometer is

$$\mathbf{E}_s \propto \mathbf{J}_p(\mathbf{J}_{\mathrm{sys,sm}}\mathbf{E}_{\mathrm{sm}} + \mathbf{J}_{\mathrm{sys,sr}}\mathbf{E}_{\mathrm{sr}}), \tag{1}$$

$$\mathbf{E}_r \propto \mathbf{J}_p(\mathbf{J}_{\mathrm{sys},r1}\mathbf{E}_{r1} + \mathbf{J}_{\mathrm{sys},r2}\mathbf{E}_{r2}), \tag{2}$$

where $\mathbf{E}_s$ is the measured sample electric field, $\mathbf{E}_r$ is the measured reference electric field, $\mathbf{J}_p$ is the rotated polarizer matrix, $\mathbf{J}_{\mathrm{sys,sm}}$, $\mathbf{J}_{\mathrm{sys,sr}}$, $\mathbf{J}_{\mathrm{sys},r1}$, and $\mathbf{J}_{\mathrm{sys},r2}$ are the system matrices for the SM, SR, R1, and R2 beams, respectively, and $\mathbf{E}_{\mathrm{sm}}$, $\mathbf{E}_{\mathrm{sr}}$, $\mathbf{E}_{r1}$, and $\mathbf{E}_{r2}$ are the respective input electric field vectors.

When, for instance, the HWP is misaligned about the azimuthal angle, it has a different effect on the $\mathbf{J}_{\mathrm{sys,sm}}$ when compared with $\mathbf{J}_{\mathrm{sys,sr}}$ because

$$\mathbf{J}_{\mathrm{sys,sm}} = \mathbf{J}_n\mathbf{J}_{n-1}\ldots\mathbf{R}_{-\theta}\mathbf{J}_{\mathrm{hwp}}\mathbf{R}_{+\theta}\mathbf{J}_1, \tag{3}$$

$$\mathbf{J}_{\mathrm{sys,sr}} = \mathbf{J}_m\mathbf{R}_{+\theta}\mathbf{J}_{\mathrm{hwp}}\mathbf{R}_{-\theta}\ldots\mathbf{J}_2\mathbf{J}_1, \tag{4}$$

the matrices do not commute, and the propagation direction changes. In these equations, $\mathbf{J}_n$ is the nth polarizing component, $\mathbf{J}_m$ is the mth polarizing component, $\mathbf{R}_{+\theta}$ and $\mathbf{R}_{-\theta}$ are the positive and negative rotational matrices, and $\mathbf{J}_{\mathrm{hwp}}$ is the HWP matrix. Even small angular misalignments can cause a large error because of a stacking effect with other misaligned components. However, because $\mathbf{J}_{\mathrm{sys},r1}$ and $\mathbf{J}_{\mathrm{sys},r2}$ follow the same principle, the effect of polarizing component misalignment is limited. Using this model for simulated sample displacements of ± 150 nm (± 1 fringe), the estimated displacement error for angles less than $\pm 0.05°$ is less than 100 pm.

Although the interferometer is balanced, meaning that only the OPD is the sample, if a polarizing component is misaligned, it will affect the SM and SR beams differently. This is particularly important for the LDPBS and the HWP. During a tolerance sensitivity analysis in ZEMAX, the splitting surface of the LDPBS contributes 30 pm/nrad of error, a tolerance that is difficult to achieve. Another problem with this interferometer is its magnified sample nonparallelism errors. Assuming a 10 mm wide sample, if one side expanded 17.5 pm, tilting the sample by 1.75 nrad, the long optical path length causes this to be magnified to 500 pm at the detector.

From numerical simulations and optical modeling, having the reference beam located within the interferometer reduces some alignment effects and nonlinearity errors. However, the trade-offs for this reduction are that the measurement is highly sensitive to component tolerances and sample tilt is indistinguishable from sample length changes. Additionally, because there is a long optical path in glass, the measurement is highly susceptible to localized birefringence errors caused by thermal and pressure fluctuations. Because of the long optical path length and the sample tilt (which may be a stability characteristic), an alternative solution was sought to simplify the double-sided, double-pass interferometer so that the optical path length would be shorter and the sample tilt could be measured.

4. Single-Pass Interferometer

Several changes were made to the double-pass design to simplify the layout, number of components, and the effects of tolerancing and alignment. The two most significant changes are that the interferometer is a single-pass instead of a double-pass configuration and that the incoming beams are spatially separated instead of being a single source. As shown in Fig. 2, the interferometer has two linearly polarized input beams with frequencies of f_1 and $f_1 + \delta f$, which come from two offset locked lasers. The idea behind this is to minimize the effect of periodic nonlinearity, which is difficult to correct for in this system. Both beams pass through a 50% beam splitter (BS), resulting in four beams, RM, SR, RR, and SM (top to bottom, Fig. 2). RM and RR interfere to create the reference signal, and SR and SM interfere to create the sample measurement signal.

Beams SR and RR follow the same path. First they pass through PBS1, QWP1, and QWP2, where the polarization state changes 90°. They then reflect off PBS2, both mirrors, and PBS1. They pass through QWP1, QWP2, and PBS2, where they then are

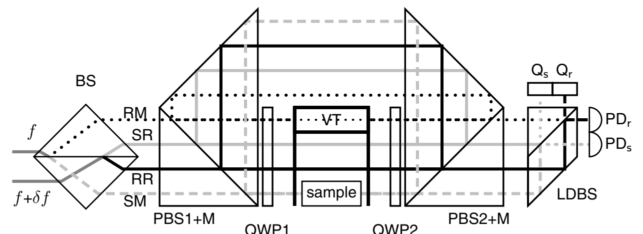

Fig. 2. Single-pass, double-sided interferometer for measuring sample length changes. The input beams have a frequency offset but are the same polarization state. The vacuum tube (VT) has extended glass flanges to keep the paths common between all four beams.

combined at the LDBS. Beam RM also follows the same exact path, except it passes through a vacuum tube (VT) twice between the two QWPs. The SM beam passes through PBS1 and QWP1, where it reflects off one side of the sample. It passes through QWP1 again and then reflects off PBS1, both mirrors, and PBS2. It then passes through QWP2, reflects off the other side of the sample, passes through QWP2 again, as well as PBS2. It then travels through the LDBS, where it interferes with beam SR. To compensate for the windows of the vacuum tube, the windows are extended through the three other beams.

The polarization states throughout the interferometer are shown in Fig. 3 to further clarify the evolution of the beam paths. It should be noted that leakage through PBS2 from the first pass can be minimized via proper alignment techniques. While it is possible to perfectly align the system, it is beneficial to slightly misalign certain components to prevent ghost reflections and unwanted beams from hitting the detector. This interferometer still exhibits some of the alignment problems based on the order of beam paths as described by Eqs. (3) and (4). However each reflection occurs the same number of times, except from the sample surfaces, at the same polarization state, which should minimize these effects.

In this interferometer, the sample signal measures sample length changes, plus changes in refractive index and interferometer motions. The reference signal measures refractive index changes and interferometer motions. However, this interferometer largely compensates for interferometer component motions because the motions are common to both the sample measurement and reference measurement. Additionally, the nonpolarizing beam splitter used as an interference element creates two equal beams for each measurement. Thus, the difference between the two signals from photodetectors PD_s and PD_r measures the sample length change while correcting for refractive index effects, and quadrant detectors (Q_s, Q_r) can measure the sample tilt versus interferometer tilt.

As with the double-pass design, this interferometer has the reference located within itself, which reduces the effect of tolerances and component alignment motions during a measurement. Using two spatially separated, nonmixed beams also means there is a minimal effect from periodic nonlinearities, which are difficult to correct because the starting point of the nonlinearity is unknown. Proper alignment techniques and coatings must be used to achieve this. When aligned properly, this eliminates the periodic nonlinearity uncertainty associated with corrective techniques (e.g., [14,15]).

The added vacuum tube allows the reference signal to follow the localized refractive index changes in the system. This eliminates the uncertainty in measuring the refractive index with a refractometer and its cross correlation to the refractive index in this interferometer and the systematic effects of using the modified Edlén formula [16].

5. Preliminary Measurements

A. System Description

The single-pass interferometer was tested in the configuration shown in Fig. 4. Instead of two offset locked lasers, a commercial laser (Zygo 2/20 Axiom) with a 20 MHz split frequency was used as the source because the offset locked laser system is still under development. The two polarization states were split by a PBS, and one state passed through a HWP to rotate its polarization state by 90°. The sample measured was an 86 nm thin film of silver coated on a 1 mm thick glass slide. The silver sample's coefficient of thermal expansion effects are negligible (approximately 4 pm), and the refractive index effects induced should be no more than the spatially separated effects. A vacuum tube was not included in these measurements because the OPD was only 86 nm and the 1 mm glass slide extends through all four beams. Last, temperature and pressure were not explicitly monitored or controlled. From previous experiments, it is known that the laboratory temperature fluctuates approximately ±1°C per 12–15 min.

The reference signal (which is the interferometer dead path) and measurement signal were measured by using two commercial photodetectors. Each signal was mixed with a common 19.975 MHz signal, which results in a signal with 25 kHz and 39.975 MHz components. The high-frequency signal was rejected

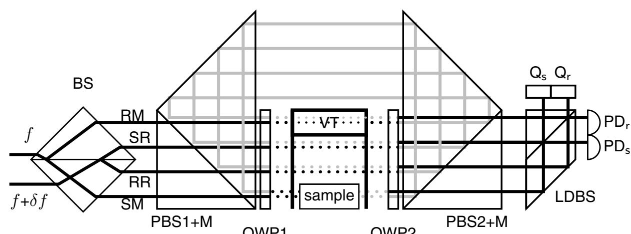

Fig. 3. Polarization schematic for the single-pass design. The black solid beams are horizontally polarized, the black dotted beams are right circularly polarized, the grey solid beams are vertically polarized, and the grey dotted beams are left circularly polarized.

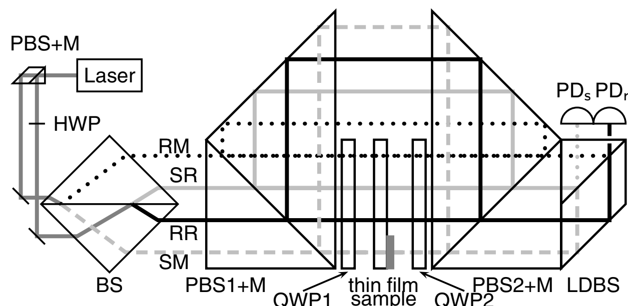

Fig. 4. Interferometer layout for measuring a zero-length sample to qualify the single-pass double-sided design. The size of PBS1 and PBS2 was 35 mm for these measurements. The total optical path after splitting is approximately 500 mm.

by using a fourth-order Butterworth low-pass filter with a cutoff frequency of 30 kHz, and the resulting signal was then amplified. Finally, the phase was measured by using a lock-in amplifier (Signal Recovery 5210) with a time constant of 300 ms and was amplified by 14 dB, which enhanced the signal resolution going into the data acquisition system (National Instruments 6025E). The phase signal was measured with a 20 kHz sampling rate every 20 ms (50 Hz) and averaged into a single data point (400 point averaging). Because of lag in the data acquisition, the effective sampling frequency was 34 Hz.

B. Repeatability Measurements

A total of 66 separate measurements of the thin-film sample were taken where the measurement period was 0.5 h. Each 0.5 h period was logged to a separate file, and the phase counter restarted before the start of the next measurement. The phase counter restarted every 30 min; thus the overall drift in the measurement was not assessed. Figure 5 shows each of the 66 measurements for the 30 min intervals. The results show that the measured length change was within 60 nm, with the majority of the values in an 8 nm spread around zero. These measurements show two distinct attributes: the observable linear drift was minimal, and the noise level was approximately the same. This is a clear indication that this interferometer produces repeatable measurements with minimal drift.

A linear fit was taken of each of the 66 measurements to determine the linear drift. Figure 6 shows the drift rate in picometers per hour on the left-hand axis for each of these measurements. The mean linear drift rate was 0.4 pm h^{-1} with a standard deviation value of 16.5 pm h^{-1} when the drifts are compared from all 66 measurements. The spread in these drift rates indicates some measurement dependency on the surrounding environment and optical setup. However, these measured values are much lower than anticipated.

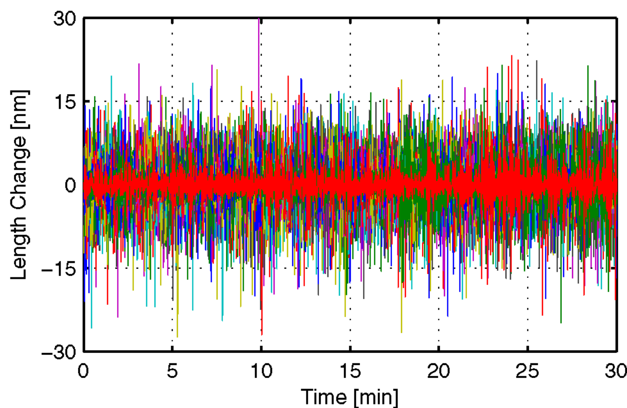

Fig. 5. (Color online) A total of 66 measurements of the silver thin-film sample overlaid on top of one another. The majority of measured length change is within an 8 nm band, and the average length change was 1.9 nm rms.

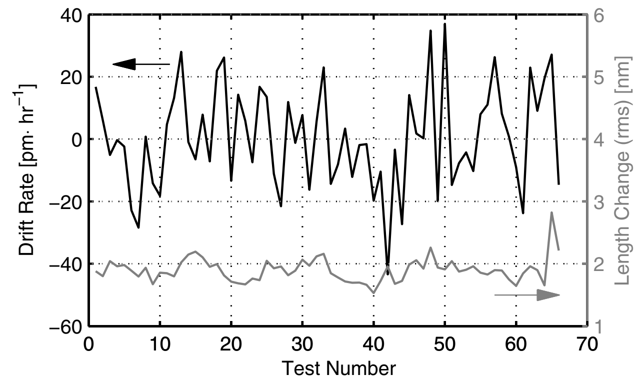

Fig. 6. Linear drift rate (left axis) and rms length change (right axis) of each of the 66, 30 min measurements. The mean drift rate was 0.4 pm h^{-1} with a standard deviation of 16.5 pm h^{-1}. The mean length change was 1.9 nm rms.

The noise level in the system was much higher than anticipated. The mean measured length change was 1.9 nm rms; the maximum of the 66 measurements was 2.8 nm rms, and the minimum was 1.5 nm rms, which is shown in Fig. 6 on the right-hand axis. This noise level is approximately 2 orders of magnitude higher than the estimated drift rate, which suggests that a true value for drift cannot be determined with noise levels this high. The high noise level is a combination of a low signal-to-noise ratio at the detector and perturbations from the surrounding environment.

C. Long-Term Measurements

The long-term drift was assessed by measuring the same 86 nm thin-film sample, using the identical signal conditioning system for intervals of 9.3 and 12.7 h. The results from these measurements are shown in Fig. 7 with the $\pm 2\sigma$ bands shown as the dashed lines. The linear drift from the 12.7 h measurement was −14.4 pm, and from the 9.3 h measurement, it was 4 pm. This is an average drift rate of

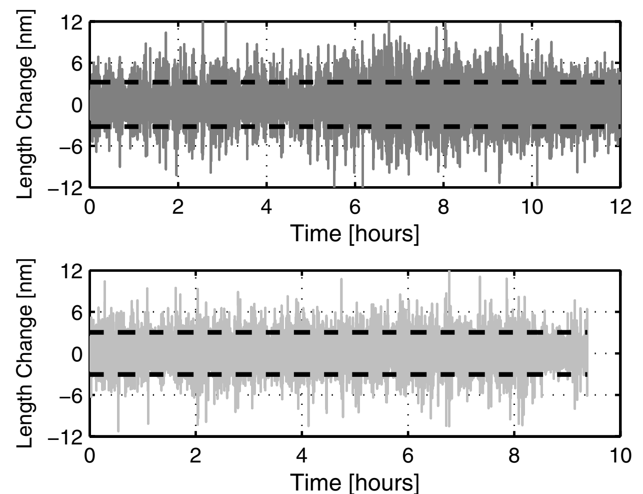

Fig. 7. Two long-term measurements over 12 and 9 h. Both measurements had a mean length change of 1.6 nm rms, and the linear drift rates were less than 1.1 pm h^{-1}.

$1.1\,\text{pm}\,\text{h}^{-1}$ for the 12.7 h measurement and $0.4\,\text{pm}\,\text{h}^{-1}$ for the 9.3 h measurement. Both of these measurements showed a length change of 1.6 nm rms.

As with the short-term repeatability experiments, the measured linear drift rate was much less than the observed noise. Both of these drift rates are in agreement with drift rate results from the short-term measurements. However, the exact drift rate is difficult to determine because of the relatively high amounts of noise.

6. Noise Sources

In these preliminary experiments, there are three main sources of the measurement noise: noise from the laser source, noise from analog electronics and data acquisition, and environmental fluctuations. Noise from the laser source and electronics was measured by placing a 45° polarizer directly in front of the laser source. The beam was then split by a 50% beam splitter and detected by using the same two detectors from the experiments. The phase difference between the two signals was processed and measured by using the same electronics and characteristics as in the experiments. Figure 8 shows the measured phase noise from the laser head. These results show that the laser, signal processing, and data acquisition contribute approximately 0.6 nm ($\pm 2\sigma$) in the thin-film experiments.

The Allan variances from the laser and electronics noise and the two long-term measurements are shown in Fig. 9. The variances show similar trends, with the laser and electronics noise at a consistent order of magnitude lower until approximately 300 s of averaging. After this time, it is unclear whether the long-term measurements start to converge with the laser and electronics. These measurements do not show the characteristic upswing that occurs in typical Allan variance figures [17]. This suggests that this interferometer is stable for long-term measurements.

The phase noise from the lock-in amplifier was assessed by using a function generator and a BNC splitter to send the same signal to the measurement and reference inputs in the lock-in amplifier. This

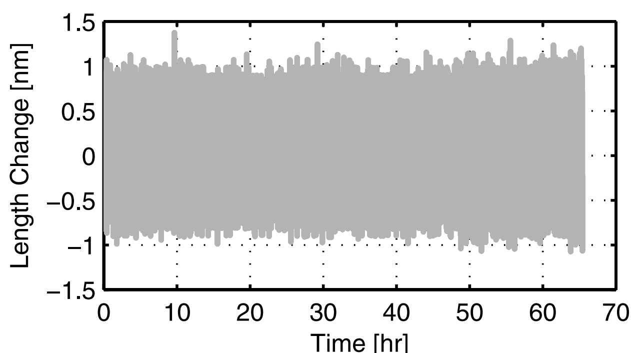

Fig. 8. Measured phase noise from the laser head, using a common polarizer and a 50% beam splitter. The phase between the two signals was measured by using the same signal processing parameters and electronics as in the thin-film measurements.

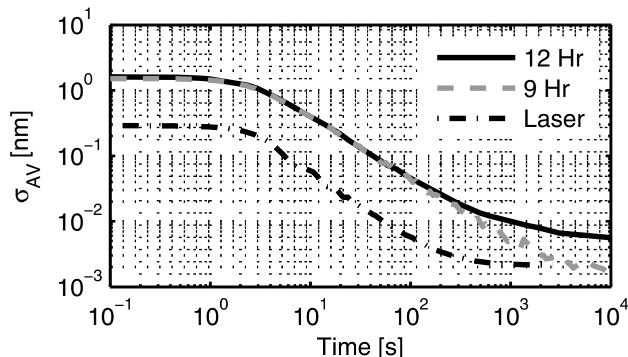

Fig. 9. Allan variances of the two long-term measurements and the phase noise (translated to nanometers) from the source. The lack of upswing over time indicates a high stability in the system.

gives an indication of whether the laser phase noise results from the frequency or intensity stability of the laser head itself or from the phase detectors and data acquisition. The measured results showed a phase noise of approximately 0.2 nm ($\pm 2\sigma$), which is three times lower than the measured laser phase noise.

One parameter that was not taken into consideration when measuring the laser phase noise was the optical power at the detector. The optics used in these measurements were not antireflection coated, which means approximately 4% of the light was lost at each of the approximately 28 glass–air transitions and 10% at each of the three mirror surfaces. Assuming $300\,\mu$W of power from the source, that leaves about $15\,\mu$W of power, assuming that all beam splitters were perfect. Additionally, a portion of the beam was lost because a pin photodiode was used. When the laser phase noise was directly measured, the measured signal was clearly visible on an oscilloscope. However, in the thin-film experiments, the signal was buried in noise due to the low optical power (approximately 1–3 μW) at the detector. The signal could be seen on the oscilloscope only after frequency mixing, low pass filtering, and then amplifying by 60 dB. This lack of power contributes to a low signal-to-noise ratio, which needs to be addressed.

The tilting effect on the sample was not addressed in this version. It is possible that the observed displacements could be attributed to rotational motions of the thin-film sample. Based on optical modeling, the sample tip and tilt sensitivity is approximately 11 and $13\,\text{pm}\,\mu\text{rad}^{-1}$, respectively. The effects of tip and tilt should be negligible compared with the observed noise level.

The temperature in the laboratory has been measured previously with ± 1°C changes every 12–15 min. The refractive index changes are largely common between both measurement and reference signals, and the sample creates only an additional 86 nm of OPD, which can be considered negligible for these experiments. What is not clear on the basis of this information is the effect of thermal gradients and localized refractive index changes in the glass. Because the temperature variations can be large,

and rapid, this can cause significant changes of the glass refractive index, which will be translated to phase noise at the detector. These issues will be evaluated in depth when improvements to the system are performed.

7. Limitations and Future Work

Currently, the suspected largest error contributors are the thermal gradients and the low signal-to-noise ratio at the detector. The high level of noise in the measurements limits the resolution for determining an overall drift pattern in the interferometer. Increasing the power at the detector and placing the system in an environmentally controlled chamber will allow the overall drift pattern to be assessed.

Several improvements to the system are currently being implemented to address the above issues and also make the system more robust. The source will be upgraded to a novel frequency and intensity stabilized, offset locked laser system that will send over 2 mW input per frequency into the interferometer. This source will also address issues with traditional offset locked systems such as relative power stability and phase noise between the two lasers. Once implemented, this should greatly increase the signal-to-noise ratio at the detector. The optical components used for the proof of principle will be replaced with fewer, custom-built combined optical assemblies and mounts, which should increase the overall stability and add much needed antireflection coatings to the air–glass transitions. Last, the system will be placed in an isolated vacuum tank, which will lead to better thermal control, pressure stability, thermal cycling, and the ability to measure under vacuum conditions.

8. Conclusions

This paper describes two different, double-sided interferometer layouts for measuring sample length changes. After numerical calculations and a tolerancing analysis, the single-pass, double-sided design was built to test its initial stability. The single-pass interferometer was tested for both short-term and long-term drift by using a 86 nm thin-film silver sample. The thin-film sample was chosen because it reduces the effect from refractive index changes while still allowing the linear drift to be measured. In a noncontrolled environment, the mean short-term and long-term linear drift estimates were approximately $1\,\mathrm{pm\,h^{-1}}$, which was much lower than anticipated.

The short-term measurements showed a fairly repeatable trend with an rms drift rate of $16.5\,\mathrm{pm\,h^{-1}}$, which is about 33 times higher than the mean drift rate. This shows some influence from the surrounding environment and dependence on optical mount stability.

Although the estimated linear drift values were higher in the short-term measurements than in the long-term measurements, the noise level prohibits a proper estimate of the actual value. Even with the measured noise level, typically, most measurements will exhibit some noticeable drift. Because these measurements did not exhibit any appreciable amount of drift, it can be inferred that this interferometer configuration is insensitive to its own stability. Another factor that skews the long-term drift to appear better is that it may be temperature-induced drift. If this is the case, the temperature fluctuations will cause positive and negative length changes to be measured, which averages out over time.

While the mean drift rates for both short- and long-term measurements were about 20 times better, the spread in the values showed the stability was better than $20\,\mathrm{pm\,h^{-1}}$.

The authors thank the Dutch IOP (projects IPT06104 and IPT004001) for supporting this research. The authors would also like to acknowledge TNO Industry & Science and the NMi Van Swinden Laboratorium BV for being partners in this research. The authors are grateful for the contributions of Dario Lo Cascio, Ad Verlaan, Joep Pijnenburg, (TNO) and Paul van Kan (NMi) in this research.

References

1. R. S. Elliott, N. Triantafyllidis, and J. A. Shaw, "Stability of crystalline solids—I: continuum and atomic lattice considerations," J. Mech. Phys. Solids **54**, 161–192 (2006).
2. Y. W. Bao, S. B. Su, J. J. Yang, L. Sun, and J. H. Gong, "Nondestructively determining local strength and residual stress of glass by Hertzian indentation," Acta Mater. **50**, 4659–4666 (2002).
3. M. Bergoglio, A. Calcatelli, M. Plassa, and P. Chen, "Gas adsorption-desorption and materials stability," Vacuum **41**, 2089–2092 (1990).
4. Y. Kuriyama, Y. Yokoyama, Y. Ishii, J. Ishikawa, and H. Makino, "Development of a new interferometric measurement system for determining the main characteristics of gauge blocks," CIRP Ann. **55**, 563–566 (2006).
5. R. Schödel, Ultra-high accuracy thermal expansion measurements with PTB's precision interferometer," Meas. Sci. Technol. **19**, 084003 (2008).
6. S. J. Bennett, "An absolute interferometric dilatometer," J. Phys. E **10**, 525–530 (1977).
7. K. P. Birch, "An automatic absolute interferometric dilatometer," J. Phys. E **20** 1387–1392 (1987).
8. M. Okaji and H. Imai, "A practical measurement system for the accurate determination of linear thermal expansion coefficients," J. Phys. E **17**, 669–673 (1984).
9. J. Suska and J. Tschirnich, "An interferometric device for precise thermal expansion measurements on bar-shaped materials," Meas. Sci. Technol. **10**, N55–N59 (1999).
10. E. G. Wolff and R. C. Savedra, "Precision interferometric dilatometer," Rev. Sci. Instrum. **56**, 1313–1319 (1985).
11. J. D. Ellis, K. Joo, A. Verlaan, J. W. Spronck, and R.-H. Munnig Schmidt, "Uncertainty considerations for interferometric stability testing," presented at Annual Meeting of the American Society for Precision Engineering 2008, Portland, Oreg., USA (23 Oct. 2008).
12. D. Ren, K. M. Lawton, and J. A. Miller, "A double-pass interferometer for measurement of dimensional changes," Meas. Sci. Technol. **19**, 025303 (2008).
13. J. D. Ellis, J. W. Spronck, and R.-H. Munnig Schmidt, "Optically balanced, multi-pass displacement interferometry for picometer stability testing," presented at Annual Meeting of

the American Society for Precision Engineering 2007, Dallas, Tex., USA (16–17 Oct. 2007).
14. W. Hou and G. Wilkening, “Investigation and compensation of the nonlinearity of heterodyne interferometers,” Precis. Eng. **14**(2), 91–98 (1992).
15. T. Eom, T. Choi, K. Lee, H. Choi, and S. Lee, “A simple method for the compensation of the nonlinearity in the heterodyne interferometer,” Meas. Sci. Technol. **13**, 222–225 (2002).
16. K. P. Birch and M. J. Downs, “An updated Edlén equation for the refractive index of air,” Metrologia **30**, 155–162 (1993).
17. J. Rutman and F. L. Walls, “Characterization of frequency stability in precision frequency sources,” Proc. IEEE **79**, 952–960 (1991).